Baohong Chen
John A. Paulson School of Engineering and Applied Sciences,
Harvard University,
Cambridge, MA 02138
e-mail: chenb@g.harvard.edu

Wenjie Sun
School of Mechanical and Precision Instrument Engineering,
Xi'an University of Technology,
Xi'an 710048, China;
State Key Laboratory for Strength and Vibration of Mechanical Structures and School of Aerospace,
Xi'an Jiaotong University,
Xi'an 710049, China
e-mail: sunwenjie2017@xaut.edu.cn

Jingjing Lu
State Key Laboratory for Mechanical Behaviour of Materials; School of Science,
Xi'an Jiaotong University,
Xi'an 710049, China
e-mail: 414857134@qq.com

Jianhai Yang
State Key Laboratory for Strength and Vibration of Mechanical Structures and School of Aerospace,
Xi'an Jiaotong University,
Xi'an 710049, China
e-mail: yangjianhai@xjtu.edu.cn

Yongmei Chen
College of Bioresources Chemical and Materials Engineering;
National Demonstration Center for Experimental Light Chemistry Engineering Education,
Shaanxi University of Science & Technology,
Xi'an 710021, China
e-mail: 913898005@qq.com

Jinxiong Zhou[1]
State Key Laboratory for Strength and Vibration of Mechanical Structures and School of Aerospace,
Xi'an Jiaotong University,
Xi'an 710049, China
e-mail: jxzhouxx@mail.xjtu.edu.cn

Zhigang Suo[1]
Kavli Institute of Bionano Science and Technology;
John A. Paulson School of Engineering and Applied Sciences,
Harvard University,
Cambridge, MA 02138
e-mail: suo@seas.harvard.edu

All-Solid Ionic Eye

We describe the materials, design, experimental measurements, and simulations of a bio-inspired all-solid tunable optical device: ionic eye. A dielectric elastomer functions as an electroactive material. An ionogel functions as an ionic conductor. Both materials are stretchable and transparent. The ionic eye achieves a ~50% relative change of the focal length, beyond that of the human eye. Our analysis also points out that the ionic eye can respond rapidly (3.6 ms) and be miniaturized in size. This all-solid deformable lens eliminates the risk of leakage of currently used encapsulated fluid lenses and can be integrated into other devices for diverse applications. [DOI: 10.1115/1.4049198]

Keywords: all-solid, tunable optics, ionic conductor, dielectric elastomer, bio-inspired, elasticity, structures

Introduction

A tunable lens changes its focal length to image objects at different distances. The human eye deforms a soft lens, whereas a camera moves a rigid one. Zooming by the rigid-body translation requires

[1]Corresponding authors.

Contributed by the Applied Mechanics Division of ASME for publication in the JOURNAL OF APPLIED MECHANICS. Manuscript received October 1, 2020; final manuscript received November 20, 2020; published online December 17, 2020. Assoc. Editor: Annie Ruimi.

space and is unsuitable for applications such as robotic vision, smartphone and laptop cameras, wearable electronics, presbyopia corrections, augmented vision, lab-on-chip devices, microscopes, and endoscopes. Intense efforts are devoted to developing deformable lenses that mimic the human eye [1–11]. However, existing deformable lenses struggle to satisfy the fast-growing demands for mobile and wearable applications [12–23]. In particular, most existing deformable lenses involve liquids or gases [1–10,12–17,24,25]; the fluids may leak and pose challenges to fabrication, integration, and reliability. Several all-solid deformable lenses have been developed, but they are bulky, complicated, or slow [19–23,26–29].

Here, we report an all-solid deformable lens, which we call the *ionic eye*. The ionic eye mimics the function of the human eye, not the anatomy and physiology. The ionic eye integrates stretchable and transparent materials of two kinds: a dielectric elastomer and an ionogel. The dielectric elastomer functions as the muscle, the ionogel as the lens and a system of nerves. We demonstrate a change in focal length (~50%) beyond that of the human eye (~30%). The ionic eye exhibits a rapid response (3.6 ms) and does not suffer gravity-induced image distortion. It is lightweight, reliable, and easy to fabricate. Our theoretical analysis shows that the ionic eye can be compact, offering possibilities to make tunable cameras for mobile and wearable devices.

The ionic eye is an electro-mechano-optical device with three functional parts: an artificial muscle to cause the deformation, a lens that changes the focal length when deformed, and a system of artificial nerves to transmit electrical signals. All parts are solid, deformable, and transparent. We implement a dielectric elastomer as the artificial muscle. A dielectric-elastomer actuator is a deformable capacitor, consisting of a sheet of dielectric elastomer sandwiched between two compliant electrical conductors [30,31]. When applying a voltage between the two conductors, the dielectric reduces its thickness and increases its area. Voltage-induced areal strains of over 1000% have been demonstrated [32,33]. Dielectric elastomers have enabled liquid deformable lenses [34–36] and metalens [37]. Compliant conductors used in these deformable lenses are electronic conductors, such as silver nanowires and carbon-based materials (e.g., carbon greases, graphene sheets, and carbon nanotubes). By contrast, the human eye is stimulated through ionic conductors: nerves. Ionic conductors such as hydrogels and ionogels have been developed recently to enable artificial muscles [38–40], skins[41], and axons [42]. A hydrogel consists of a polymer network and water and can be stretchable, transparent, and water-retaining [43–46]. An ionogel consists of a polymeric network and an ionic liquid and can be made stretchable, transparent, and nonvolatile [40,47]. Indeed, these ionic conductors are much more transparent and stretchable than electronic conductors such as silver nanowires, graphene sheets, and carbon nanotubes [38]. Ionogels show the potential for replacing these conductors in some existing compact active liquid lenses [35]. Although the conductivity of ionic conductors is typically lower than that of the electronic conductors, the ionic conductors retain their conductivity under large stretches and over many cycles [38]. They readily function as artificial nerves to transmit high-speed electrical signals over long distances [38,42]. Hydrophobic ionogel conductors have been expanded to enhance the environmental resistivity [48–50]. Here, we fabricate the lens and the artificial nerves using an ionogel that we previously developed [40].

The ionic eye mimics the human eye (Fig. 1). In the human eye, the ciliary body contracts to focus on a nearby object, deforming the lens to decrease the focal length (Fig. 1(*a*)). The ciliary body relaxes to focus on a distant object, flattening the lens to increase the focal length (Fig. 1(*b*)) [51–53]. We design the ionic eye by sandwiching a dielectric-elastomer sheet between a lens-shaped ionic conductor and a disk-shaped ionic conductor (Fig. 1(*c*)). The two ionic conductors connect, through thin lines of ionic conductors and metallic electrodes, to an external electronic circuit. The interface between the ionic conductor and the metallic conductor contains an electrical double layer (EDL) with a large capacitance in series with a small dielectric-elastomer capacitance (Fig. 1(*d*)). When the metallic electrodes are subjected to an applied voltage, the voltage drops negligibly across the EDL (less than 1 V) and mostly across the dielectric elastomer [38,40]. The small voltage across the EDL will not cause electrolysis, and the large voltage across the dielectric elastomer causes it to reduce in thickness and expand in the area. The off

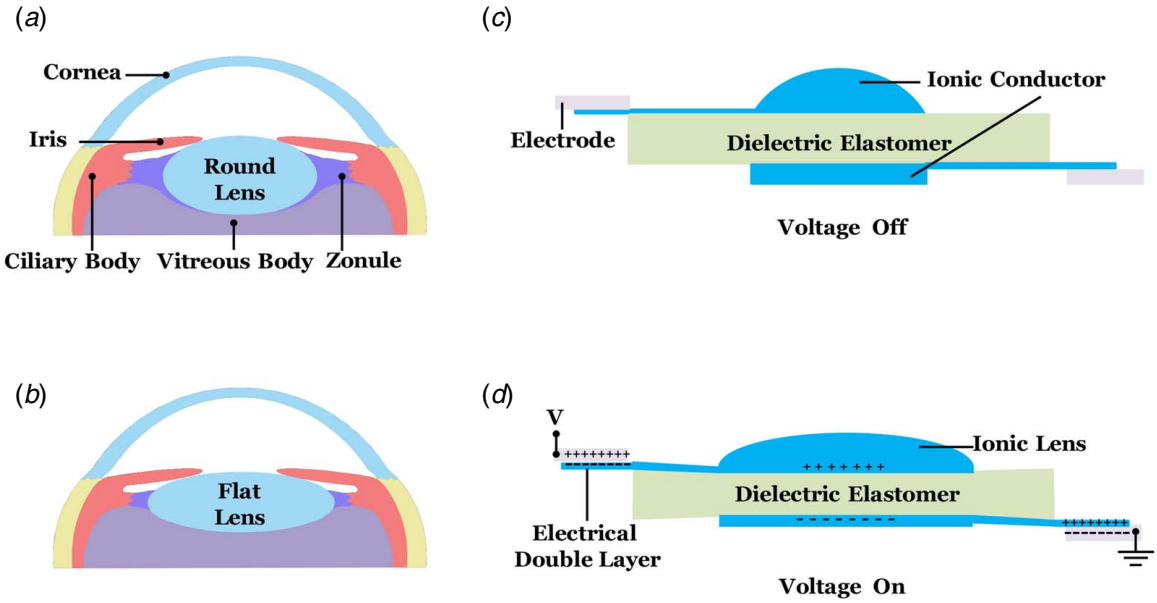

Fig. 1 Cross-sectional views of the human eye and the ionic eye. (*a*) When the ciliary body in the human eye contracts, the lens curves, and the focal length becomes shorter. (*b*) When the ciliary body relaxes, the lens flattens, and the focal length becomes longer. (*c*) The ionic eye consists of a dielectric-elastomer sheet, a lens-shaped ionic conductor, and a disk-shaped ionic conductor. The lens and the disk are connected via lines of the ionic conductor to two metallic electrodes. (*d*) When the two electrodes are subjected to a voltage, ions of the opposite polarities spread on the two faces of the dielectric elastomer, the dielectric elastomer reduces in thickness and expands in area, and the lens flattens.

and on voltage states shift the profiles of the lens between large and small curvatures. Continuously changing the voltage, the ionic eye can reproduce every intermediate form of the human eye. The preliminary prototype of the ionic eye shows remarkable deformations and excellent transparency (See Video 1 available in the Supplemental Materials on the ASME Digital Collection).

Fabrications and Measurements of the Ionic Eye

We fabricate the ionic eye using a simple process (Fig. 2). A plano-convex ionogel lens is obtained by pouring a pre-gel solution into a glass or plastic mold. The mold is a cavity in the shape of a spherical cap, where the base diameter is D, and the depth is h. We then seal the solution with a glass or plastic plate transparent to ultraviolet light and irradiate ultraviolet light into the sealed solution for two hours. A disk-shaped ionogel is fabricated similarly by using a mold with a disk-shaped cavity, where the diameter is 14 mm and the depth is 0.3 mm. The artificial muscle needs to be strong to actuate the ionic lens. Thus, a three-layer circular dielectric elastomer (VHB 4910, 3M^{TM}, 1 mm thick per layer) of diameter A is radially prestretched λ times the original diameter using a specialized stretcher (see Video 2 available in the Supplemental Materials on the ASME Digital Collection) and is fixed by two rigid frames of inner diameter B. On the two faces of this fixed dielectric, we directly attach the lens-shaped and the disk-shaped ionogels. The ionogels and the dielectric elastomer remain adhered in subsequent experiments (Figs. 2(*f*) and 2(*g*)). The ionogel lens and disk are connected to the aluminum electrodes of the power source through thin ionogel lines (0.3 mm thick and 3 mm wide). An ionic eye is fabricated with parameters of $D = 14$ mm, $h = 4.5$ mm, $A = 31$ mm, $\lambda = 3$ and $B = 93$ mm (Figs. 2(*f*)–2(*h*)). A photo shows a flower observed through this ionic eye (Fig. 2(*i*)).

We apply a cyclic voltage to realize dynamic imaging. On one side of the ionic eye, we place three objects: the Arabic number "1" in black, an artificial limb in yellow, and a person in blue, at distances of 10 cm, 1 m, and 2.5 m, respectively (Fig. 3(*a*)). On the other side of the ionic eye, we place a digital camera with a fixed focal length at a fixed distance. The photograph of the object number "1" is evident on the camera before applying a voltage to the ionic eye. A sinusoidal voltage (amplitude, 12 kV; frequency, 1/8 Hz) is used to deform the dielectric elastomer. The electric field in the elastomer is $\sim 10^8$ V m^{-1}, well below the electrical breakdown strength of the material [31].

As the voltage cycles, the ionic eye changes its focal length, and the objects come in and out of focus (see Video 3 available in the Supplemental Materials on the ASME Digital Collection). When the voltage is zero, the number "1," the closest object to the ionic eye, is in focus, but the other items are not (Fig. 3(*b*)). As the voltage increases, the image of number "1" becomes blurred, while the other objects gradually become apparent, first the yellow artificial limb, then the person in blue, and even the windows (Fig. 3(*c*)). Once the voltage peaks, everything in view is out of focus because the object that could be in focus is beyond the edge of the room (Fig. 3(*d*)). As the voltage decreases, items come into focus again in reverse order (Fig. 3(*e*)).

The transmittance of the ionogel is high; the average transmittance of a 10-mm thick ionogel is 97% for the light of wavelengths between 380 and 720 nm [40]. However, the clarity and sharpness of the images can be affected by other factors. Examples include the

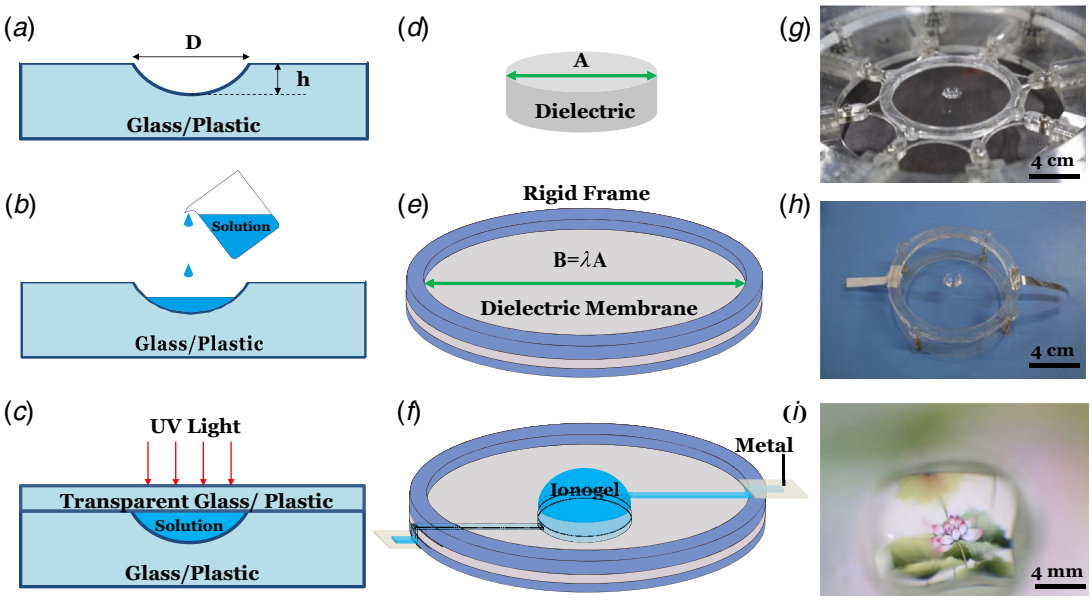

Fig. 2 The fabrication of an ionic eye. (*a*) A glass or plastic mold has a cavity in the shape of a spherical cap with the base diameter $D = 14$ mm and the height $h = 4.5$ mm. (*b*) Pour a pre-gel solution (the mixture of the monomer, ionic liquid, cross-linker, and catalyst) into the mold. (*c*) Seal the mold with a transparent plate of glass or plastic. Under the radiation of the ultraviolet light for two hours, the solution turns into an ionogel with a covalent polymer network. A circular disk of the ionogel is prepared by changing the mold with a disk-shaped cavity. (*d*) A dielectric-elastomer sheet of the circular shape, the diameter $A = 31$ mm, and the thickness 3 mm is in the undeformed state. (*e*) Stretch the dielectric sheet radially to $\lambda = 3$ times the original diameter and fix it with two rigid frames. (*f*) Attach the lens-shaped and the disk-shaped ionogels on the two surfaces of the dielectric elastomer. Both ionogels are connected to metallic electrodes (aluminum) through the thin ionogel lines (section area: 0.3 mm × 3 mm). (*g*) The photo of the radial stretcher, the stretched dielectric membrane, and the ionic lens. (*h*) The photo of the ionic eye. (*i*) A photo is taken through the ionic eye. The setup shown in (*f*) (D = 14 mm and $h = 4.5$ mm) is directly mounted on the screen of a cell phone (Vivo Xplay 2013). The distance between the cell phone screen and the ionic lens's bottom surface is estimated as ~5–10 cm. A digital camera (Canon EOS 5D) shots the photo ~20 cm above the ionic lens, inside the room during the day. The diameter of the flower on the screen is estimated as ~2 cm.

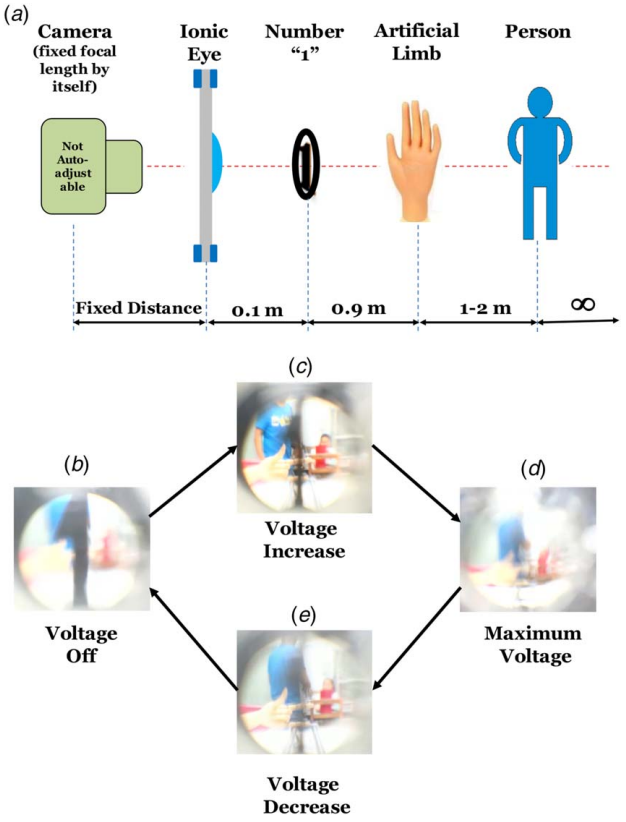

Fig. 3 The ionic eye changes the focal length. (*a*) The digital camera (Canon EOS 5D) with a fixed focal length, an ionic eye, and several objects is placed at fixed positions. (*b*)–(*e*) Frames of a video recorded by the camera (Video 3). As the sinusoidal voltage (amplitude: 12 kV; frequency 1/8 Hz) is applied to the ionic lens cycles, the objects come into and out of focus. The focus voltages of the number, the artificial limb, and the person are estimated as 0 V, ~11 kV, and ~11.5 kV, respectively. The artificial limb and the person are probably in the same depth of field. Thus, they almost become apparent at the same time. When the maximum voltage is reached, the depth of field is beyond the room's dimension (~4 m). Thus, all objects become blur again. Illumination condition: lights are turned on in the room. (Color version online.)

lens's optical aberrations, the lens's smoothness, air bubbles and other defects inside the lens, and the lab's illumination environment. Systematically resolving these issues goes beyond the scope of this paper.

The voltage-induced change of the focal length is readily visualized (Fig. 4, see Video 4 available in the Supplemental Materials on the ASME Digital Collection). We place an ionic eye on a tank of water's outer wall and direct two parallel laser beams to the ionic eye. The ionic eye, the tank's wall, and the water are all refractive so that the two laser beams bend and intersect. As the applied voltage changes, the ionic eye deforms, and the two laser beams change the amount of bending.

We measure the change of the ionic eye's focal length as a function of the applied voltage (Fig. 5). We place an ionic eye in the air, shine a beam of parallel light to the base of the lens, and observe the light spot on a screen ahead of the lens's curved side. When the screen moves relative to the ionic eye, the spot on the screen changes size. The distance between the screen and the base center of the lens when the spot is the smallest is the measured focal length. In the absence of a voltage, the measured focal length of the ionic lens is 17.4 ± 0.65 mm. For a plano-convex lens, one can calculate the focal length from the expression $f = R_L/(n-1)$, where R_L is the radius of the lens's curvature, and n is the refractive index of the ionogel [54]. For a lens in the shape of a spherical cap

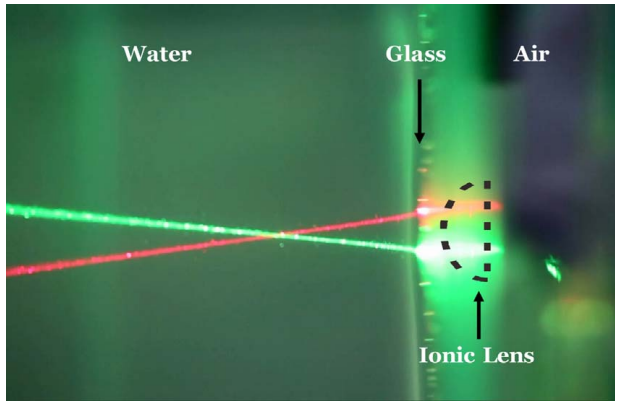

Fig. 4 The visualization of ionic eye's focal length changing. Two beams of parallel light pass through the ionic lens (in the air) and cross in the water (Video 4).

with a base diameter $D = 14$ mm (error, 1.2%) and a height $h = 4.5$ mm (error, 4.89%), the geometry gives the radius of curvature $R_L = (h^2 + D^2/4)/2\,h = 7.7 \pm 0.3$ mm. The measured refractive index of the ionogel is $n = 1.46 \pm 0.06$, comparable to that of silicon oil ($n_o = 1.4$). The calculated focal length is $f_0 = 16.94 \pm 1.93$ mm, which is very close to the measured result (3% error). When the ionic eye is actuated, the larger the voltage, the flatter the lens, and the longer the focal length (Fig. 5). The largest focal length is $f_{\max} = 25.6 \pm 1.3$ mm. Thus, the ionic eye can change the focal length by $47\% \pm 7.6\%$, which exceeds that of human eyes (~30% from Ref. [34]).

The electromechanical deformation of the ionic eye is further analyzed through a finite element method. The result suggests a nonlinear relation between the relative change of focal length (y) and the applied voltage (x). We fit the relation as $y = 0.0024 \times x^4 - 0.063 \times x^3 + 0.64 \times x^2 - 1.8 \times x + 1.1$. The profile of the finite element model (FEM) changes remarkably (Fig. 5(*a*)). Meanwhile, we obtain the profile of the ionic lens experimentally (Figs. 5(*c*) and 5(*d*)). Carbon grease is smeared on the ionic lens to provide a better reflection for the laser sensor. For a larger and softer lens, the profile changes more significantly. For the smaller lens, the profile changes less than the prediction of simulations. This profile may be due to the poor adhesion between the ionic lens and the dielectric elastomer.

The response time of the ionic eye may be limited by the elastomer and the gel's viscoelasticity and inertia. The elastomer used in this work (VHB) exhibits significant viscoelastic behavior and is unsuitable for testing response over a wide range of frequencies. It has been shown that the response time improves when a less viscous elastomer is used, such as silicone rubbers [36]. Here, we estimate the theoretical limit of the response time set by the inertia. The masses of the ionogel lens and the dielectric elastomer are $m_i = \rho_i V_i$ and $m_d = \rho_d V_d$, where ρ_i and ρ_d are the densities, and V_i and V_d are the volumes of the ionogel and dielectric, respectively. The ionogel and the elastomer's effective stiffnesses are $k_i \sim Y_i\, H_{i\max}$ and $k_d \sim Y_d\, H_d$, where Y_i and Y_d are the elastic moduli of the ionogel and the dielectric, respectively. $H_{i\max}$ is the maximum height of the lens, and H_d is the thickness of the dielectric. The frequency of the fundamental mode of resonance is $\omega = (k/\mathrm{m})^{1/2}$, setting a time scale $\tau = 1/\omega$. Taking representative values $\rho_i = \rho_d = 10^3 \mathrm{kgm}^{-3}$, $V_i = 1.25\pi \times 10^{-7}$ m^3, $V_d = 1.47\pi \times 10^{-8}$ m^3, $Y_i \sim 10^3$ N m^{-2}, $Y_d \sim 10^5$ N m^{-2}, $H_{i\max} = 4.5 \times 10^{-3}$ m, and $H_d = 3 \times 10^{-4}$ m, we find that $\tau \sim [(m_i + m_d)/(k_i + k_d)]^{1/2} \approx 3.6$ ms. Such a short response time is sufficient for mobile and wearable devices.

We also perform a theoretical analysis to probe the possibility of miniaturizing the ionic eye. In this analysis, we ignore the ionogel and consider the constraint due to the ionogel on the dielectric's deformation by increasing the dielectric's modulus. The elastic

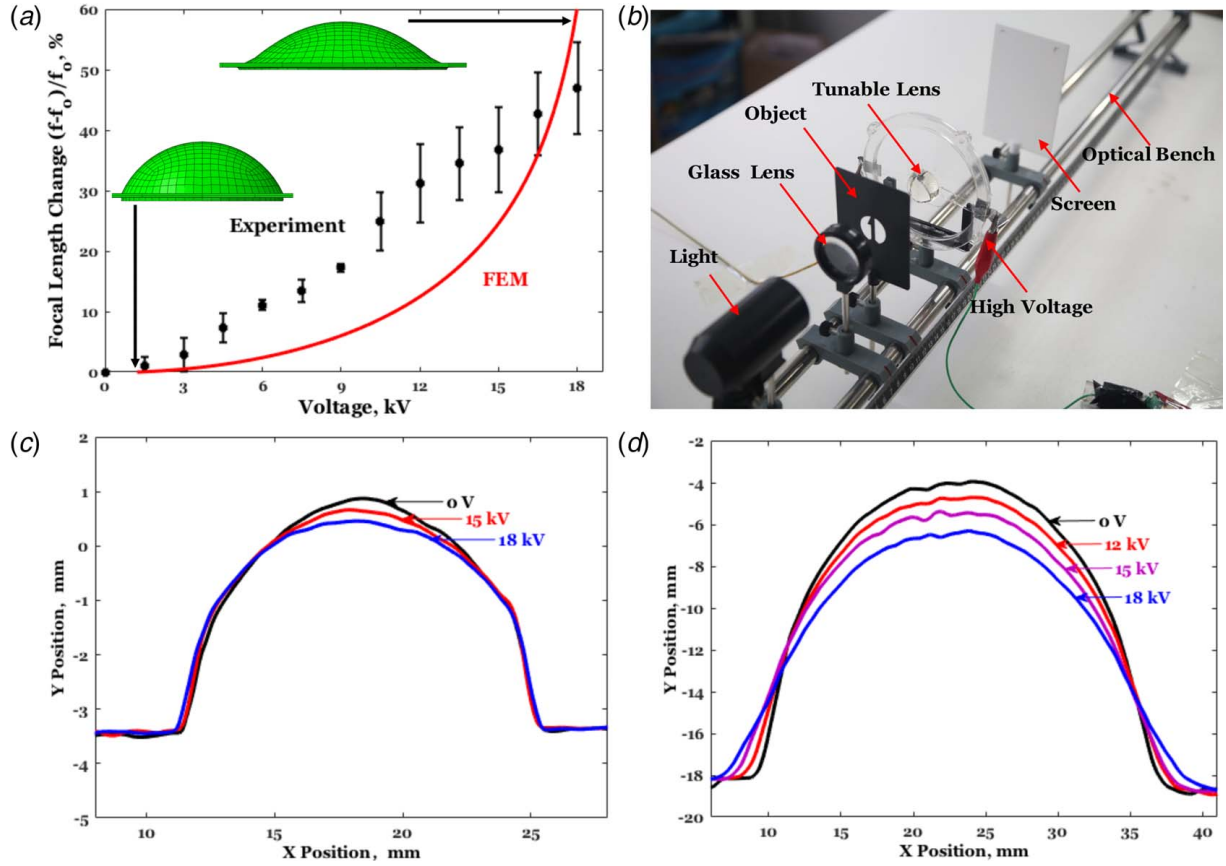

Fig. 5 (*a*) The relative change of the focal length of an ionic eye ($D = 14$ mm and $h = 4.5$ mm) is recorded as a function of the voltage. The ionic eye's focal length is $f_o = 17.4 \pm 0.65$ mm in the undeformed state and achieves the maximum focal length $f_{max} = 25.6 \pm 1.3$ mm in the deformed state. The largest change of the focal length is $47\% \pm 7.6\%$, beyond that of the human eye (~30%). The FEM simulation shows the nonlinear relation between the relative change of the focal length and the applied voltage. Insert: deformations of the model in ABAQUS. (*b*) The setup used for measuring the focal length. The measured profiles of (c) a smaller ionic lens ($D = 14$ mm and $h = 4.5$ mm) and (*d*) a bigger and softer ionic lens ($D = 30$ mm and $h = 14$ mm) under constant voltages in experiments.

modulus of the ionogel is typically 3 kPa [40], and the elastic modulus of the dielectric is in the range of 0.1–3 MPa [30]. We take the dielectric's shear modulus as 45 kPa in the active region ($R < D$) to equal the total effective stiffness. We also assume the deformation of dielectric elastomer is equal-biaxial and thus adopt a simple model. Figure 6 plots the stretch (λ) of the dielectric elastomer versus the applied electrical field for various frame/lens diameter ratios, B/D. If $B/D = 1$, deformation is fully constrained. The deformation increases as B/D increases but levels off when B/D is greater than 6. The solid red line depicts our design at $B/D = 6.6$. The maximum deformation, where λ is approximately 4.7, is limited by the electrical breakdown (~150 MV m^{-1}), as shown by the dashed red line in Fig. 6. Our theoretical result indicates that the diameter ratio can be reduced to $B/D = 2$, an optimal value that can generate fairly large deformation ($\lambda \sim 4.5$). Given specific geometric shapes, the height of the lens h is reduced along with the base diameter D. Therefore, the thickness of the dielectric membrane is reduced, as well as the voltage. The whole ionic eye can be miniaturized to a compact size, implying an opportunity for devices in small spaces.

The adhesion between ionic conductors and dielectrics will affect the lifetime of the devices. A method was recently proposed to measure the debond energy between two highly stretchable materials by calculating the bilayer structure's energy release rate [55]. We adopt this method, follow the same protocol, and measure the debond energy for bilayer structures of ionogel and VHB. We cut the VHB into ribbons with dimensions of $70 \times 10 \times 1$ mm^3 and attach a $20 \times 10 \times 3$ mm^3 ionogel on the center of the VHB. The gauge length of the bilayer structure is 40 mm, defined by the distance between the tensile machine's two clamps. A $3 \times 10 \times 0.1$ mm^3 crack is made between ionogel and VHB at one end of the interface. The crack propagates when the bilayer is stretched to 1.43 times the original length (Fig. 7). This critical stretch changes with the ionogel thickness, but the debond energy does not [55]. In this experiment, the debond energy is ~1 J m^{-2}. Such debond energy is relatively low. During our experiments, the ionic lens always stays adhered to on VHB. Still, the low adhesion energy affects the sufficient deformation of the ionic lens, thus reducing the focal length's maximum change.

Recent advances have achieved gel–elastomer and gel–metal adhesions of high toughness, transparency, and stretchability or conductivity [56]. The interfacial fracture energy of ionic conductors could be vastly enhanced to ~1 kJ m^{-2} [57] using chemical anchors. Bulk modification of both ionic conductors and elastomers can also provide strong adhesion and a sharp optical interface [58]. Topological entanglement among long polymer chains, ionic conductors, and elastomers could achieve reversible adhesions [59,60]. Lastly, subwavelength molecular staples could perhaps provide both a transparent optical interface and the tough adhesion to integrate soft materials [61]. These techniques are expected to prevent the delamination of dissimilar soft materials in the ionic eye during actuation.

Both hydrophobic and hydrophilic ionic liquids have numerous varieties [62,63]. Using appropriate ionic liquids, the ionogel lens can be made to survive over a broad range of temperatures, from ~−100 °C to ~300 °C [64–66]. Ionogel lenses can satisfy some

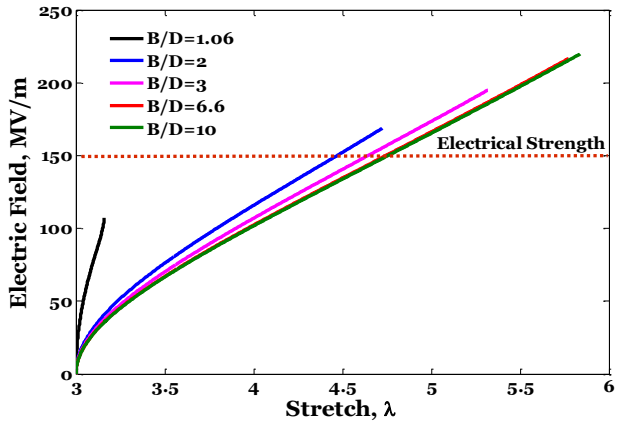

Fig. 6 The size of the rigid frame affects the tuning range of the ionic eye. The electric field is plotted as a function of the radial stretch for several ratios of the frame's inner diameter over the base diameter of the undeformed ionic eye, *B/D*. The prestretch of the dielectric elastomer is 3. When *B/D* > 6, a further increase of the frame's size no longer increases the tuning range of the ionic eye. Before the electrical breakdown, the setup with *B/D* ~ 2 can reach the human eye's tuning range. (Color version online.)

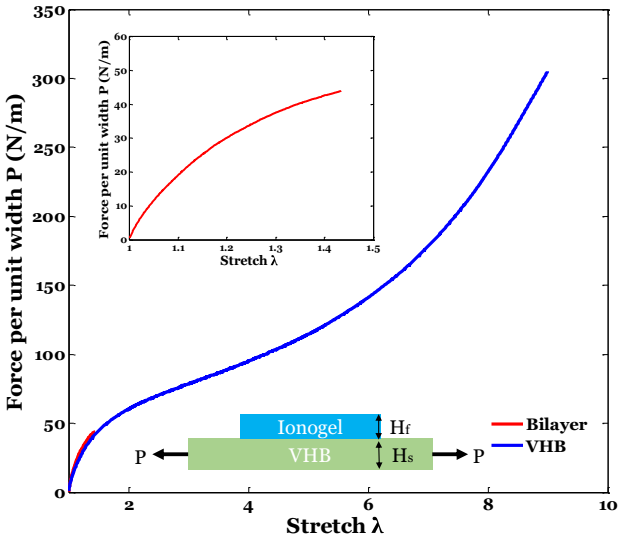

Fig. 7 The force–stretch curves of the bilayer structure (in red) and VHB (in blue). The debond energy between the ionogel and the VHB is ~1 J m^{-2}. The thicknesses of ionogel and VHB are $H_f = 3$ mm and $H_s = 1$ mm, respectively. The critic force for the crack propagation in the bilayer is 44 N m^{-1}, and the critic stretch is 1.43. (Color version online.)

particular uses, such as devices in outer space or exposed to sun and rain. Even though the mechanical properties of VHB elastomers change with the temperature, other elastomers can be used over a relatively broad temperature range from subzero to hundreds of degrees Celcius. For example, one can use polydimethylsiloxane (PDMS) from −40 to 150 °C [67,68]. With that said, at room temperature and after millions of actuations and months of exposure to air, conditions representative of a typical application, a dielectric-elastomer actuator with ionogels as conductors still performs well [40].

At room temperature, the thermal expansion coefficients of the ionic liquid ([C_2mim][$EtSO_4$]) and the elastomer (VHB 4910) in this work are 5.5×10^{-4} K^{-1} [69] and 1.8×10^{-4} K^{-1} (3M^{TM}), respectively. The weight of polyacrylic acid polymer chains is only 5.5% of the weight of ionogel in this work. Thus, thermal expansion coefficients of both ionogels and VHB elastomers are small and comparable. When a tough and transparent adhesion is made between the gel and the elastomer, the thermal expansion mismatch can be accommodated by the interface's high toughness (~1000 J m^{-2}) due to the softness and the stretchability of both materials. In practice, the ionic eye's possible failure modes are the electric breakdown of dielectrics (short circuit), the electric field concentration along the edges of the ionic lens, the aging of dielectrics, and the debond between the lens and the elastomer due to the fatigue of the interface.

In summary, the ionic eye offers new opportunities for designers of tunable optics. We report an all-solid tunable lens activated through a dielectric elastomer and ionogels. The ionic eye varies the focal length beyond that of the human eye. To mimic the human eye's systematic functions, more sensors and circuits need to be integrated. The ionic eye is able to cooperate with ionic sensors and circuits and be integrated into ionotronic devices. Moving beyond the human eye, ionic lenses could also be arranged in an array with other actuation principles to design powerful tunable optics, such as arthropod eyes for robots [70,71]. All of these opportunities require the advantages of stretchable and transparent solid-state ionic conductors.

Experimental Sections

Fabrication of the ionogel: 1-Ethyl-3-methylimidazolium ethylsulfate ([C_2mim][$EtSO_4$], Linzhou Keneng Material Technology Co.), acrylic acid (AA, Tianjin Yongsheng Chemical Co.), poly(ethylene glycol) diacrylate (PEGDA, Sigma-Aldrich Co.), and α-ketoglutaric acid (Aladdin Industrial Co.) are chosen as the ionic liquid, the monomer of the polymer network, the cross-linker, and the initiator, respectively. Dissolve the monomer into the ionic liquid at 1 mol L^{-1} and add the cross-linker and the initiator at 0.6 mol% and 1 mol% of the monomer, respectively. After mixing, transfer the solution into the glass, plastic, or rubber molds. The glass mold is a concave contact lens mold [72–74] and used to make the smaller lens ($D = 14$ mm, $h = 4.5$ mm). The plastic or rubber molds for the larger lens ($D = 30$ mm, $h = 14$ mm) are widely used polycarbonate or silicon semispherical molds for foods or epoxy models (purchased on Amazon.com). The plastic mold for the fabrication of circular ionogels (diameter: 14 mm; thickness: 0.3 mm) is cut by a laser cutter (Versa Laser VLS2.30, Universal Laser Systems). The commercial molds are relatively precise; thus, the estimated error of fabrication is <1%. The molds cut by the laser cutter have an estimated systematic error of ~5%. Then, put the sealed solution into an ultraviolet light chamber (power: 50 W, wavelength: 365 nm, SCIENTZ 03-II, Ningbo Scientz Biotechnology Co.) for 2 h. After the assembly, the undeformed sizes of ionic lenses measured in Figs. 5(*c*) and 5(*d*) by laser sensor are $D = 14.17$ mm and $h = 4.28$ mm for the smaller lens and $D = 29.31$ mm and $h = 14.41$ mm for the larger lens. Thus, the errors of D are 1.2% for the smaller lens and 2.3% for the larger lens, and the errors of h are 4.89% for the smaller lens and 2.93% for the larger lens.

The stretcher and the prestretch: The stretcher is manufactured in-house, consisting of nine gears and eight gear racks made of acrylic plastic (poly(methyl methacrylic), PMMA) shown in Video 2. Three layers of sticky VHB elastomers are carefully stacked together. The VHB elastomer is mounted and clamped at the end of acrylic gear racks and prestretched to a specific area before constrained by a pair of acrylic circles, as shown in Fig. 2(*g*).

Minimizations of the device's defects: Ionic liquids are heated up to 80 °C to remove the water for 12 h in a thermostatic chamber. To eliminate the air bubbles in the ionic lens, the air is evacuated from the precursor in a desiccator (0.29 psi). To avoid air bubbles visible to the naked eye between two layers of VHB elastomers, a hard rubber brayer (such as the Testrite 24B) is used to roll toward one

direction while attaching one layer on the other. To avoid visible air bubbles at the lens–elastomer interface, the lens is bent by a tweezer and attached gradually to the elastomer.

The assembly of the device: To better adhere the lens and the elastomer, we use nitrogen gas to dry both surfaces before attaching them. Without treatments of materials and additions of adhesives, the VHB elastomer itself is sticky, and the gel is also somewhat tacky. The adhesion between ionogels and VHB elastomers is due to the Van der Waals interactions. When the applied voltage is less than 18 kV, the bonding is sufficient for presented deformations within the testing period. Longer time and higher frequency actuation require a more robust bonding between gels and elastomers. We indicate several methods to make better adhesions in the main text. The connection between gels and electrodes is caused by direct contact in this work. The excellent bonding between gels and metallic electrodes can be achieved using chemical anchors [57] or molecular staples [61]. We have not tried these methods for this work.

Optical properties of ionic conductors: The refractive index of the ionic liquid is measured using the 2W Abbe's refractometer (Shanghai Optical Instrument Company), and $n_l = 1.467 \pm 0.001$. The refractive index of ionogel is calculated according to Snell's law. Radiate a beam of light into a block of ionogel, the incident angle is 30 ± 1 deg, and the refractive angle is 20 ± 1 deg; thus, $n_s \approx 1.46 \pm 0.06$ (Snell's law: $n_{21} = \sin\theta_1/\sin\theta_2 = \sin 30 \text{ deg}/\sin 20 \text{ deg}$).

Profile measurements of the solid lens: A two-dimensional laser displacement sensor (LJ-G200, Keyence) shines an array of the laser beam to the surface of objects and measures the relative height in a cross section of the object. The item is ahead of the laser sensor 200 ± 1 mm, and the standard length of the laser array in this distance is 70 mm.

The adhesion measurement of stretchable bilayer structures: A tensile machine (CMT6503, MTS) is used to measure the bonding between the ionogel and the VHB elastomer in the air and at room temperature: load cell, 100 N; strain rate, 0.0125 s^{-1}. When the crack starts propagating, the recorded force drops slightly. The corresponding stretch and force are critical values. Figure 7 shows the bilayer's force–stretch curve (in red) is plotted up to the critical stretch. The areas under force–stretch curves of both the bilayer and the substrate are integrated up to the critic stretch to calculate the debond energy. We assume that the local stretches at both the bonded region and the debond region are uniform, given the film is softer than the substrate. According to the energy release rate calculation [55], the debond energy equals the difference between the two areas.

The Theoretical Section

A circular dielectric-elastomer actuator consists of an active region and a passive region. During the actuation, the elastic energy is restored in both the active and passive regions, but the electrical polarization energy is collected in the active region.

We use the Gent model [75] to describe the elastic energy density of the dielectric elastomer, in the form of $W^{\text{elas}} = -(\mu J_{lim}/2)\ln[1 - (2\lambda^2 + \lambda^{-4} - 3)/J_{lim}]$, where μ is the shearing modulus, J_{lim} is the parameter related to the locking strain, and λ is the equal-biaxial stretch. The electrical energy density powered to the active region is $W^{elec} = \varepsilon E^2/2$, where ε is the permittivity of dielectric elastomer, and E is the electric field. According to the variations of the free energy, the governing equation of the active region is $\lambda s + \varepsilon E^2 = \mu(\lambda^2 - \lambda^{-4})/[1 - (2\lambda^2 + \lambda^{-4} - 3)/J_{lim}]$, where s is the nominal stress in the active region. This formulation couples the stress, stretch, and electric field together. Combining the force balance and boundary conditions, relations between any two of three quantities can be described.

Considering the inhomogeneous deformation in the passive region, the force balance formulates that $\partial s_1/\partial R - (s_1 - s_2)/R = 0$, where s_1 and s_2 are the nominal stresses in the radial and circular directions, respectively, and R is the radial distance of a mass particle away from the center of the actuator. The boundary conditions are $s_1|_{R=D} = s|_{R=D}$, $\lambda_2|_{R=D} = \lambda|_{R=D}$, and $\lambda_2|_{R=B} = \lambda_{pre} = 3$. We use the following parameters in the calculations: $\mu = 45$ kPa, $J_{lim} = 500$, $\varepsilon = 4.16 \times 10^{-11} \text{Fm}^{-1}$.

The Simulation Section

We apply the above-mentioned method into a commercial finite element software (ABAQUS) and code the free energy functions for both the dielectric and the ionogel in the user-supplied subroutine (UMAT) to simulate the nonlinear electromechanical behavior of the ionic eye [76]. The equal-biaxial prestretch of the dielectric elastomer is 3, and the outer boundary is constrained after the prestretch. The bonding between the ionogel and the dielectric is prescribed by the Tie constrain in the software. We choose the C3D8H element type for both the dielectric and the ionogel. The parameters used in the calculation are $\mu_{\text{DE}} = 32$ kPa, $\mu_{\text{Gel}} = 1$ kPa, $J_{lim} = \infty$, $\varepsilon = 3 \times 10^{-11}$ F m^{-1}, $B/D = 6.6$, and $h/D = 0.3$.

Acknowledgment

B. Chen and Z. Suo acknowledge the support of NSF MRSEC (DMR-14-20570). W. Sun acknowledges the support of the State Key Laboratory for Strength and Vibration of Mechanical Structures (SV2018-KF-08). J. Yang acknowledges the support of the Research Fund for the Doctoral Program of Higher Education of China (Grant No. 20130201120049). Y. Chen acknowledges the support of the National Natural Science Foundation of China (Grant No. 11674263). J. Zhou acknowledges the support of NSFC (Grant Nos. 11472210 and 11372239).

Conflict of Interest

There are no conflicts of interest.

Data Availability Statement

The data sets generated and supporting the findings of this article are obtainable from the corresponding author upon reasonable request. The authors attest that all data for this study are included in the paper.

Nomenclature

f = focal length of the lens
h = height of the spherical cap
k = stiffness
n = refractive index
m = mass
A = diameter of the dielectric before stretched
B = inner diameter of the rigid frame
D = base diameter of the spherical cap
E = electric field
H = height or thickness
R = radial Lagrangian coordinate of the material particle
S = nominal stress
V = volume
W = elastic energy density
Y = Young's modulus
J_{lim} = locking strain
R_L = radius of curvature of the lens
ε = permittivity of the dielectric
λ = stretch
μ = shear modulus
ρ = density
τ = response time
ω = frequency of the resonance

References

[1] Kuiper, S., and Hendriks, B., 2004, "Variable-Focus Liquid Lens for Miniature Cameras," Appl. Phys. Lett., **85**(7), pp. 1128–1130.
[2] Lee, J. K., Choi, J. C., Jang, W. I., Kim, H.-R., and Kong, S. H., 2012, "Electrowetting Lens Employing Hemispherical Cavity Formed by Hydrofluoric Acid, Nitric Acid, and Acetic Acid Etching of Silicon," Jpn. J. Appl. Phys., **51**(6S), p. 06FL05.
[3] Jung, I., Xiao, J., Malyarchuk, V., Lu, C., Li, M., Liu, Z., Yoon, J., Huang, Y., and Rogers, J. A., 2011, "Dynamically Tunable Hemispherical Electronic Eye Camera System With Adjustable Zoom Capability," Proc. Natl. Acad. Sci. U. S. A., **108**(5), pp. 1788–1793.
[4] Tang, S. K., Stan, C. A., and Whitesides, G. M., 2008, "Dynamically Reconfigurable Liquid-Core Liquid-Cladding Lens in a Microfluidic Channel," Lab Chip, **8**(3), pp. 395–401.
[5] Mao, X., Lin, S.-C. S., Lapsley, M. I., Shi, J., Juluri, B. K., and Huang, T. J., 2009, "Tunable Liquid Gradient Refractive Index (L-GRIN) Lens With Two Degrees of Freedom," Lab Chip, **9**(14), pp. 2050–2058.
[6] Aljasem, K., Werber, A., Seifert, A., and Zappe, H., 2008, "Fiber Optic Tunable Probe for Endoscopic Optical Coherence Tomography," J. Opt. A: Pure Appl. Opt., **10**(4), p. 044012.
[7] Duparré, J., Wippermann, F., Dannberg, P., and Bräuer, A., 2008, "Artificial Compound Eye Zoom Camera," Bioinspiration Biomimetics, **3**(4), p. 046008.
[8] Zhu, D., Li, C., Zeng, X., and Jiang, H., 2009, "Hydrogel-Actuated Tunable-Focus Microlens Arrays Mimicking Compound Eyes," Proceedings of TRANSDUCERS 2009-2009 International Solid-State Sensors, Denver, CO, June 21–25, IEEE, pp. 2302–2305.
[9] Dong, L., Agarwal, A. K., Beebe, D. J., and Jiang, H., 2006, "Adaptive Liquid Microlenses Activated by Stimuli-Responsive Hydrogels," Nature, **442**(7102), p. 551.
[10] Shi, J., Stratton, Z., Lin, S.-C. S., Huang, H., and Huang, T. J., 2010, "Tunable Optofluidic Microlens Through Active Pressure Control of an Air–Liquid Interface," Microfluid. Nanofluid., **9**(2–3), pp. 313–318.
[11] Liang, D., Lin, Z.-F., Huang, C.-C., and Shih, W.-P., 2014, "Tunable Lens Driven by Dielectric Elastomer Actuator With Ionic Electrodes," Micro Nano Lett., **9**(12), pp. 869–873.
[12] Xu, S., Ren, H., Lin, Y.-J., Moharam, M. J., Wu, S.-T., and Tabiryan, N., 2009, "Adaptive Liquid Lens Actuated by Photo-Polymer," Optics Express, **17**(20), pp. 17590–17595.
[13] Lee, S. W., and Lee, S. S., 2007, "Focal Tunable Liquid Lens Integrated With an Electromagnetic Actuator," Appl. Phys. Lett., **90**(12), p. 121129.
[14] Malouin, B. A., Jr, Vogel, M. J., Olles, J. D., Cheng, L., and Hirsa, A. H., 2011, "Electromagnetic Liquid Pistons for Capillarity-Based Pumping," Lab Chip, **11**(3), pp. 393–397.
[15] Berge, B., and Peseux, J., 2000, "Variable Focal Lens Controlled by an External Voltage: An Application of Electrowetting," European Physical J. E, **3**(2), pp. 159–163.
[16] Binh-Khiem, N., Matsumoto, K., and Shimoyama, I., 2008, "Polymer Thin Film Deposited on Liquid for Varifocal Encapsulated Liquid Lenses," Appl. Phys. Lett., **93**(12), p. 124101.
[17] Nguyen, N.-T., 2010, "Micro-Optofluidic Lenses: A Review," Biomicrofluidics, **4**(3), p. 031501.
[18] Pfeifer, R., Lungarella, M., and Iida, F., 2012, "The Challenges Ahead for Bio-inspired'soft'robotics," Commun. ACM, **55**(11), pp. 76–87.
[19] Beadie, G., Sandrock, M., Wiggins, M., Lepkowicz, R., Shirk, J., Ponting, M., Yang, Y., Kazmierczak, T., Hiltner, A., and Baer, E., 2008, "Tunable Polymer Lens," Optics Express, **16**(16), pp. 11847–11857.
[20] Schuhladen, S., Petsch, S., Liebetraut, P., Müller, P., and Zappe, H., 2013, "Miniaturized Tunable Imaging System Inspired by the Human Eye," Opt. Lett., **38**(20), pp. 3991–3994.
[21] Lee, S.-Y., Tung, H.-W., Chen, W.-C., and Fang, W., 2006, "Thermal Actuated Solid Tunable Lens," IEEE Photonics Technol. Lett., **18**(21), pp. 2191–2193.
[22] Koyama, D., Isago, R., and Nakamura, K., 2012, "Ultrasonic Variable-Focus Optical Lens Using Viscoelastic Material," Appl. Phys. Lett., **100**(9), p. 091102.
[23] Ren, H., Fox, D. W., Wu, B., and Wu, S.-T., 2007, "Liquid Crystal Lens With Large Focal Length Tunability and Low Operating Voltage," Optics Express, **15**(18), pp. 11328–11335.
[24] Wei, K., Domicone, N. W., and Zhao, Y., 2014, "Electroactive Liquid Lens Driven by an Annular Membrane," Opt. Lett., **39**(5), pp. 1318–1321.
[25] López, C. A., Lee, C.-C., and Hirsa, A. H., 2005, "Electrochemically Activated Adaptive Liquid Lens," Appl. Phys. Lett., **87**(13), p. 134102.
[26] Nam, S., Yun, S., Yoon, J. W., Park, S., Park, S. K., Mun, S., Park, B., and Kyung, K.-U., 2018, "A Robust Soft Lens for Tunable Camera Application Using Dielectric Elastomer Actuators," Soft Rob., **5**(6), pp. 777–782.
[27] Kamali, S. M., Arbabi, E., Arbabi, A., Horie, Y., and Faraon, A., 2016, "Highly Tunable Elastic Dielectric Metasurface Lenses," Laser Photonics Rev., **10**(6), pp. 1002–1008.
[28] Zou, Y., Zhang, W., Chau, F. S., and Zhou, G., 2015, "Miniature Adjustable-Focus Endoscope With a Solid Electrically Tunable Lens," Optics Express, **23**(16), pp. 20582–20592.
[29] Choi, D.-S., Shimoga, G., Shin, E.-J., and Kim, S.-Y., 2019, "Self-Deformable Varifocal Lens Based on Electroactive Gel," Proceedings of Nano-, Bio-, Info-Tech Sensors and 3D Systems III, International Society for Optics and Photonics, Denver, CO, p. 1096911.
[30] Carpi, F., De Rossi, D., Kornbluh, R., Pelrine, R. E., and Sommer-Larsen, P., 2011, *Dielectric Elastomers as Electromechanical Transducers: Fundamentals, Materials, Devices, Models and Applications of an Emerging Electroactive Polymer Technology*, Elsevier, New York.
[31] Pelrine, R., Kornbluh, R., Pei, Q., and Joseph, J., 2000, "High-Speed Electrically Actuated Elastomers With Strain Greater Than 100%," Science, **287**(5454), pp. 836–839.
[32] Zhao, X., and Suo, Z., 2010, "Theory of Dielectric Elastomers Capable of Giant Deformation of Actuation," Phys. Rev. Lett., **104**(17), p. 178302.
[33] Keplinger, C., Li, T., Baumgartner, R., Suo, Z., and Bauer, S., 2012, "Harnessing Snap-Through Instability in Soft Dielectrics to Achieve Giant Voltage-Triggered Deformation," Soft Matter, **8**(2), pp. 285–288.
[34] Carpi, F., Frediani, G., Turco, S., and De Rossi, D., 2011, "Bioinspired Tunable Lens With Muscle-Like Electroactive Elastomers," Adv. Funct. Mater., **21**(21), pp. 4152–4158.
[35] Shian, S., Diebold, R. M., and Clarke, D. R., 2013, "Tunable Lenses Using Transparent Dielectric Elastomer Actuators," Optics Express, **21**(7), pp. 8669–8676.
[36] Maffli, L., Rosset, S., Ghilardi, M., Carpi, F., and Shea, H., 2015, "Ultrafast All-Polymer Electrically Tunable Silicone Lenses," Adv. Funct. Mater., **25**(11), pp. 1656–1665.
[37] She, A., Zhang, S., Shian, S., Clarke, D. R., and Capasso, F., 2017, "Large Area Electrically Tunable Lenses Based on Metasurfaces and Dielectric Elastomer Actuators," arXiv preprint arXiv:1708.01972.
[38] Keplinger, C., Sun, J.-Y., Foo, C. C., Rothemund, P., Whitesides, G. M., and Suo, Z., 2013, "Stretchable, Transparent, Ionic Conductors," Science, **341**(6149), pp. 984–987.
[39] Chen, B., Bai, Y., Xiang, F., Sun, J. Y., Mei Chen, Y., Wang, H., Zhou, J., and Suo, Z., 2014, "Stretchable and Transparent Hydrogels as Soft Conductors for Dielectric Elastomer Actuators," J. Polym. Sci., Part B: Polym. Phys., **52**(16), pp. 1055–1060.
[40] Chen, B., Lu, J. J., Yang, C. H., Yang, J. H., Zhou, J., Chen, Y. M., and Suo, Z., 2014, "Highly Stretchable and Transparent Ionogels as Nonvolatile Conductors for Dielectric Elastomer Transducers," ACS Appl. Mater. Interfaces, **6**(10), pp. 7840–7845.
[41] Sun, J. Y., Keplinger, C., Whitesides, G. M., and Suo, Z., 2014, "Ionic Skin," Adv. Mater., **26**(45), pp. 7608–7614.
[42] Yang, C. H., Chen, B., Lu, J. J., Yang, J. H., Zhou, J., Chen, Y. M., and Suo, Z., 2015, "Ionic Cable," Extreme Mech. Lett., **3**, pp. 59–65.
[43] Calvert, P., 2009, "Hydrogels for Soft Machines," Adv. Mater., **21**(7), pp. 743–756.
[44] Sun, J.-Y., Zhao, X., Illeperuma, W. R., Chaudhuri, O., Oh, K. H., Mooney, D. J., Vlassak, J. J., and Suo, Z., 2012, "Highly Stretchable and Tough Hydrogels," Nature, **489**(7414), p. 133.
[45] Zhao, X., 2014, "Multi-Scale Multi-Mechanism Design of Tough Hydrogels: Building Dissipation Into Stretchy Networks," Soft Matter, **10**(5), pp. 672–687.
[46] Bai, Y., Chen, B., Xiang, F., Zhou, J., Wang, H., and Suo, Z., 2014, "Transparent Hydrogel With Enhanced Water Retention Capacity by Introducing Highly Hydratable Salt," Appl. Phys. Lett., **105**(15), p. 151903.
[47] Susan, M. A. B. H., Kaneko, T., Noda, A., and Watanabe, M., 2005, "Ion Gels Prepared by In situ Radical Polymerization of Vinyl Monomers in an Ionic Liquid and Their Characterization as Polymer Electrolytes," J. Am. Chem. Soc., **127**(13), pp. 4976–4983.
[48] Gao, Y., Shi, L., Lu, S., Zhu, T., Da, X., Li, Y., Bu, H., Gao, G., and Ding, S., 2019, "Highly Stretchable Organogel Ionic Conductor With Extreme Temperature Tolerance," Chemistry Mater., **31**(9), pp. 3257–3264.
[49] Cao, Y., Tan, Y. J., Li, S., Lee, W. W., Guo, H., Cai, Y., Wang, C., and Tee, B. C.-K., 2019, "Self-Healing Electronic Skins for Aquatic Environments," Nature Electronics, **2**(2), p. 75.
[50] Sinawang, G., Kobayashi, Y., Zheng, Y., Takashima, Y., Harada, A., and Yamaguchi, H., 2019, "Preparation of Supramolecular Ionic Liquid Gels Based on Host–Guest Interactions and Their Swelling and Ionic Conductive Properties," Macromolecules, **52**(8), pp. 2932–2938.
[51] Atchison, D. A., and Smith, G., 2000, *Optics of the Human Eye*, Butterworth-Heinemann, Oxford.
[52] Oyster, C. W., 1999, *The Human Eye*, Sinauer, Sunderland, MA.
[53] Koretz, J. F., and Handelman, G. H., 1988, "How the Human Eye Focuses," Scientific American, **259**(1), pp. 92–99.
[54] Feynman, R. P., Leighton, R. B., and Sands, M., 2013, *The Feynman Lectures on Physics, Desktop Edition Volume I, Vol. 1*, Basic Books, Caltech.
[55] Tang, J., Li, J., Vlassak, J. J., and Suo, Z., 2016, "Adhesion Between Highly Stretchable Materials," Soft Matter, **12**(4), pp. 1093–1099.
[56] Yang, J., Bai, R., Chen, B., and Suo, Z., 2019, "Hydrogel Adhesion: A Supramolecular Synergy of Chemistry, Topology, and Mechanics," Adv. Funct. Mater., **30**(2), p. 1901693.
[57] Yuk, H., Zhang, T., Lin, S., Parada, G. A., and Zhao, X., 2016, "Tough Bonding of Hydrogels to Diverse Non-Porous Surfaces," Nat. Mater., **15**(2), p. 190.
[58] Liu, Q., Nian, G., Yang, C., Qu, S., and Suo, Z., 2018, "Bonding Dissimilar Polymer Networks in Various Manufacturing Processes," Nat. Commun., **9**(1), p. 846.
[59] Gao, Y., Wu, K., and Suo, Z., 2019, "Photodetachable Adhesion," Adv. Mater., **31**(6), p. 1806948.
[60] Yang, J., Bai, R., Li, J., Yang, C. H., Yao, X., Liu, Q., Vlassak, J., Mooney, D., and Suo, Z., 2019, "Design Molecular Topology for Wet-Dry Adhesion," ACS Appl. Mater. Interfaces, **11**(27), pp. 24802–24811.
[61] Chen, B., Yang, J., Bai, R., and Suo, Z., 2019, "Molecular Staples for Tough and Stretchable Adhesion in Integrated Soft Materials," Adv. Healthcare Mater., **8**(19).

[62] Werner, S., Haumann, M., and Wasserscheid, P., 2010, "Ionic Liquids in Chemical Engineering," Annual Rev. Chem. Biomolecular Eng., **1**(1), pp. 203–230.
[63] Le Bideau, J., Viau, L., and Vioux, A., 2011, "Ionogels, Ionic Liquid Based Hybrid Materials," Chem. Soc. Rev., **40**(2), pp. 907–925.
[64] Huddleston, J. G., Visser, A. E., Reichert, W. M., Willauer, H. D., Broker, G. A., and Rogers, R. D., 2001, "Characterization and Comparison of Hydrophilic and Hydrophobic Room Temperature Ionic Liquids Incorporating the Imidazolium Cation," Green Chem., **3**(4), pp. 156–164.
[65] MacFarlane, D. R., Golding, J., Forsyth, S., Forsyth, M., and Deacon, G. B., 2001, "Low Viscosity Ionic Liquids Based on Organic Salts of the Dicyanamide Anion," Chem. Commun., (16), pp. 1430–1431.
[66] Galiński, M., Lewandowski, A., and Stępniak, I., 2006, "Ionic Liquids as Electrolytes," Electrochim. Acta, **51**(26), pp. 5567–5580.
[67] Gohil, S., Suhail, S., Rose, J., Vella, T., and Nair, L., 2017, "Polymers and Composites for Orthopedic Applications," Mater. Bone Disorders, Elsevier, pp. 349–403.
[68] Radhakrishnan, T., 2006, "Thermal Degradation of Poly (Dimethylsilylene) and Poly (Tetramethyldisilylene-co-Styrene)," J. Appl. Polym. Sci., **99**(5), pp. 2679–2686.
[69] Larriba, M., García, S., García, J. n., Torrecilla, J. S., and Rodríguez, F., 2011, "Thermophysical Properties of 1-Ethyl-3-Methylimidazolium 1, 1, 2, 2-Tetrafluoroethanesulfonate and 1-Ethyl-3-Methylimidazolium Ethylsulfate Ionic Liquids as a Function of Temperature," J. Chem. Eng. Data, **56**(9), pp. 3589–3597.
[70] Song, Y. M., Xie, Y., Malyarchuk, V., Xiao, J., Jung, I., Choi, K.-J., Liu, Z., Park, H., Lu, C., and Kim, R.-H., 2013, "Digital Cameras With Designs Inspired by the Arthropod eye," Nature, **497**(7447), p. 95.
[71] Li, Z., and Xiao, J., 2015, "Strain Tunable Optics of Elastomeric Microlens Array," Extreme Mech. Lett., **4**, pp. 118–123.
[72] Maulvi, F. A., Choksi, H. H., Desai, A. R., Patel, A. S., Ranch, K. M., Vyas, B. A., and Shah, D. O., 2017, "pH Triggered Controlled Drug Delivery From Contact Lenses: Addressing the Challenges of Drug Leaching During Sterilization and Storage," Colloids Surfaces B: Biointerfaces, **157**(1), pp. 72–82.
[73] Chiou, J.-C., Hsu, S.-H., Huang, Y.-C., Yeh, G.-T., Liou, W.-T., and Kuei, C.-K., 2017, "A Wirelessly Powered Smart Contact Lens With Reconfigurable Wide Range and Tunable Sensitivity Sensor Readout Circuitry," Sensors, **17**(1), p. 108.
[74] Yao, H., Marcheselli, C., Afanasiev, A., Lähdesmäki, I., and Parviz, B., 2012, "A Soft Hydrogel Contact Lens With an Encapsulated Sensor for Tear Glucose Monitoring," Proceedings of 2012 IEEE 25th International Conference on Micro Electro Mechanical Systems (MEMS), Paris, France, Jan. 29–Feb. 2.
[75] Gent, A., 1996, "A New Constitutive Relation for Rubber," Rubber Chem. Technol., **69**(1), pp. 59–61.
[76] Zhao, X., and Suo, Z., 2008, "Method to Analyze Programmable Deformation of Dielectric Elastomer Layers," Appl. Phys. Lett., **93**(25), p. 251902.